LEHIGH UNIVERSITY

Internalized Gap Junctions are Degraded by Autophagy

379/B406

Rachael M. Kells[1], John T. Fong[1], Anna M. Gumpert[1,3], Jutta Marzillier[1], Michael Davidson[2], Matthias M. Falk[1]

[1]Department of Biological Sciences, Lehigh University, Bethlehem, PA 18015; [2] Department of Biological Science, Florida State University, Tallahassee, FL, 32310; [3] Center for Translational Medicine, Thomas Jefferson University, Philadelphia, PA, 19107

Abstract

Direct intercellular communication mediated by gap junction (GJ) channels is a hallmark of normal cell and tissue physiology. In addition, GJs significantly contribute to physical cell-cell adhesion. Clearly, these cellular functions require precise modulation. Typically, GJs represent arrays of hundreds to thousands of densely packed channels, each one assembled from two half-channels (connexons), that dock head-on in the extracellular space to form the channel arrays (termed GJ plaques) that link neighboring cells together. Interestingly, docked GJ channels cannot be separated into connexons under physiological conditions, posing potential challenges to GJ channel renewal and physical cell-cell separation. We described previously that cells continuously, and effectively after treatment with natural inflammatory mediators, internalize their GJs in a process that closely resembles clathrin-mediated endocytosis, thus enabling these critical cellular functions (Piehl et al., 2007; Gumpert et al., 2008; Baker et al., 2008; Gilleron et al., 2008). GJ internalization generates characteristic cytoplasmic double-membrane vesicles, described and termed earlier annular GJs (AGJs) or connexosomes. Here, using expression of the major fluorescent-tagged GJ protein, connexin 43 (Cx43-GFP/YFP/mApple) in HeLa cells, as well as analysis of endogenously expressed Cx43, ultrastructural analyses, confocal colocalization microscopy, pharmacological and molecular biological RNA-interference approaches depleting cells of key-autophagic proteins, we provide compelling evidence that GJs, following internalization, are degraded by autophagy. The ubiquitin-binding protein p62/SQSTM1 (sequestosome 1) was identified in targeting internalized GJ vesicles to autophagic degradation. While previous studies identified proteasomal and endo-/lysosomal pathways in Cx43 and GJ degradation, our study provides novel molecular and mechanistic insights into an alternative GJ degradation pathway. Its recent link to health and disease (Hesketh et al., 2010) lends additional importance to this GJ degradation mechanism and to autophagy in general.

Plasma membrane GJs internalize to form cytoplasmic double-membrane GJ vesicles (Annular Gap Junctions [AGJs] or connexosomes) that subsequently are degraded

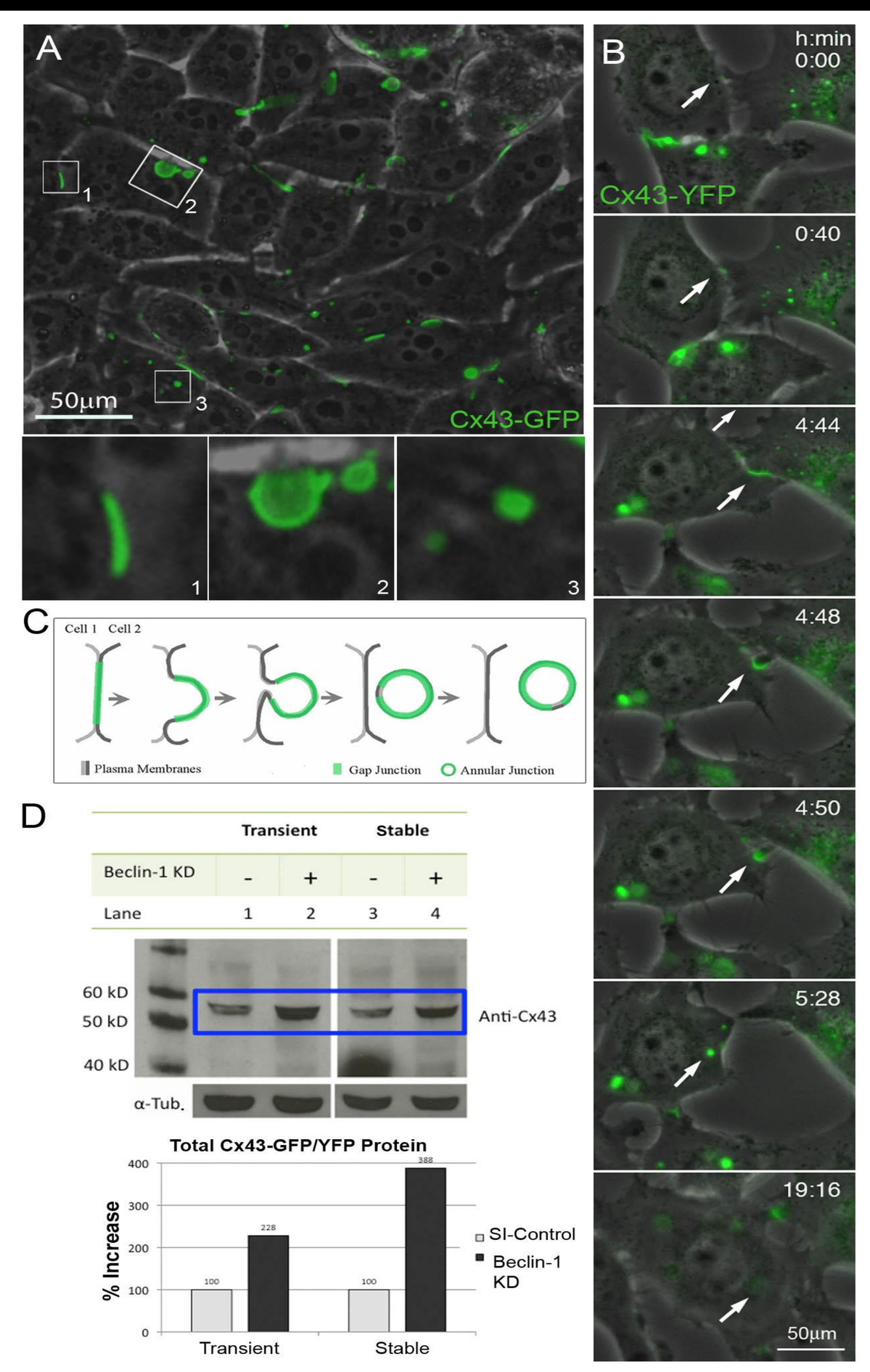

Figure 1: Plasma membrane GJs internalize to form cytoplasmic double-membrane GJ vesicles (termed annular gap junctions [AGJs] or connexosomes) that subsequently are degraded. (**A**) HeLa cells transfected with Cx43-GFP efficiently express and assemble GJs in the adjacent plasma membranes of transfected cells after overnight expression (visible as green fluorescent lines and puncta, such as the one shown in insert 1). Over time, GJs bulge inward (insert 2), detach from the plasma membrane and form cytoplasmic AGJ vesicles or connexosomes (insert 3). (**B**) Selected still-images of a time-lapse recording of stably transfected Cx43-YFP expressing HeLa cells covering over 19 hours (2 minute image intervals), showing the formation of a GJ plaque, its endocytic internalization into the cytoplasm of one of the previously coupled cells, and final degradation of the generated AGJ vesicle, indicated by the loss of its fluorescence (marked with arrows). Combined phase contrast and fluorescence images are shown in (A) and (B) and in Movie 1. (**C**) Schematic representation depicting the progressive stages of GJ internalization. For ultrastructural and additional analyses of internalizing GJs see reference 8. (**D**) Western blot analyses of total Cx43-GFP, or Cx43-YFP protein in transiently and stably expressing HeLa cells 72 hours after Beclin1 protein was depleted by RNAi-oligonucleotide transfection. SI-control cells were transfected with a scrambled non-targeting RISC-activating control oligonucleotide. Cx43-GFP/YFP was detected by probing with polyclonal anti-Cx43 antibodies. After stripping, blots were re-probed with anti-α-tubulin antibodies as a loading control. Normalized quantitative analyses revealed a two to three-fold increase of Cx43-GFP/YFP in the Beclin1-KD over SI control cells.

AGJ vesicles robustly colocalize with lysosomal and autophagosomal marker proteins, but only inefficiently with endosomal markers

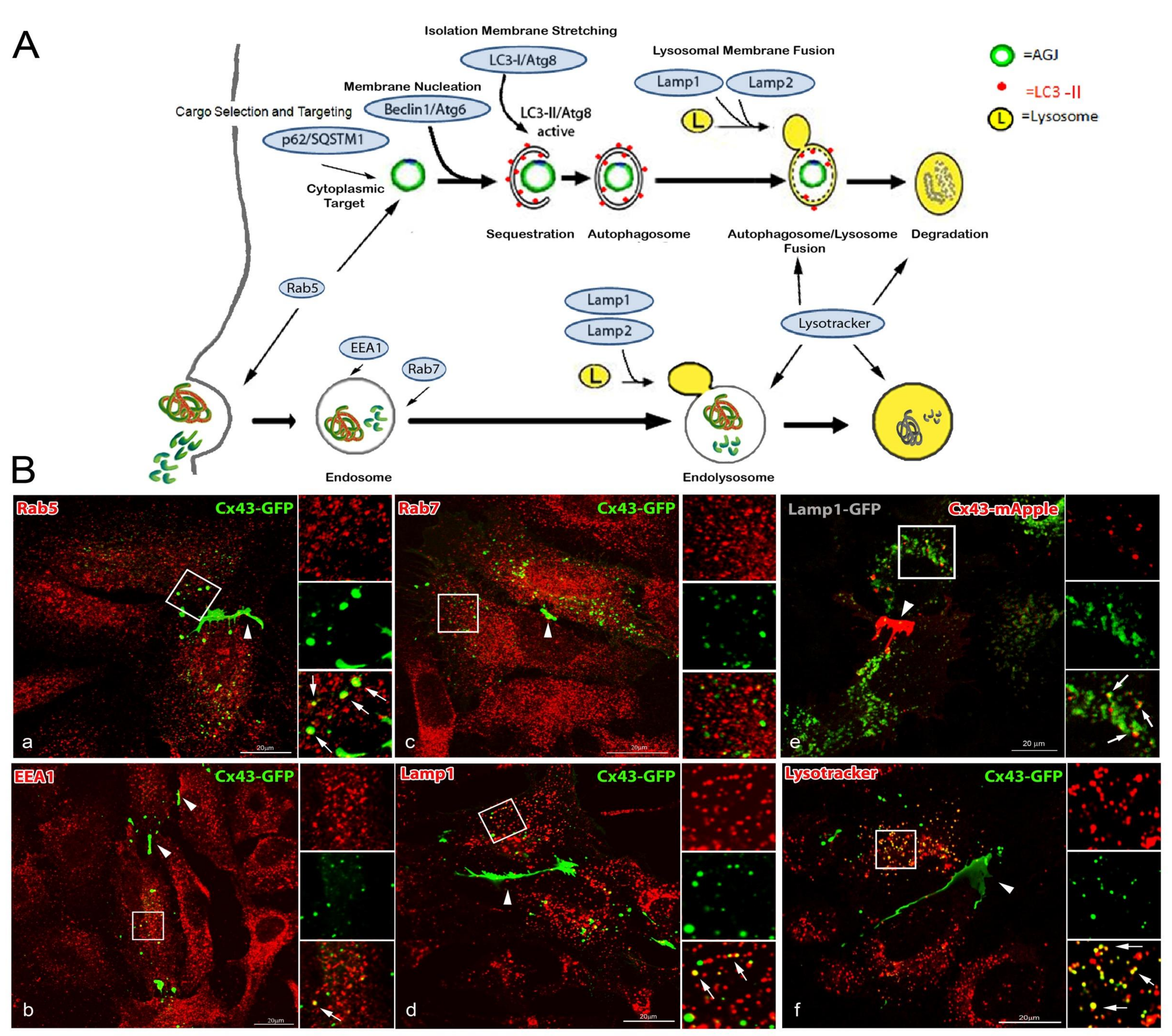

Figure 2: AGJ vesicles robustly colocalize with lysosomal and autophagosomal markers but only insignificantly with endosomal markers. (**A**) Schematic representation of phago-/lysosomal and endo-/lysosomal cellular degradation pathways and respective marker proteins (highlighted with blue shading) that have been investigated in this study. (**B**) Cx43-GFP or Cx43-mApple expressing HeLa cells were either labeled with antibodies specific for endosomal and lysosomal marker proteins (a-d), co-transfected with Lamp-1-cerulean (e), or stained with the acidophilic fluorescent probe, LysoTracker Red (f). Representative merged confocal fluorescence images obtained 20-24 hours after transfection are shown. Individual and merged fluorescence signals of the boxed areas are shown at higher magnification on the right. Robust colocalization of vesicular Cx43 was observed with lysosomal markers (Lamp-1, Lamp-1-cerulean, and LysoTracker, panels d-f, as indicated by yellow, the resulting color of overlaying red and green emission signals), but only insignificantly with endosomal markers (EEA1 and Rab7, panels b, c). A notable colocaliztion of Cx43-GFP was also observed with the GTP-binding protein Rab5 (panel a), described to be involved in early steps of endocytosis (uncoating of clathrin-coated vesicles), and in targeting cytoplasmic cargo to autophagic degradation (see text). Representative colocalizing vesicles are marked with arrows; GJs are marked with arrowheads.

Ultrastructural analysis reveals multiple stages of phagophore formation around AGJ vesicles

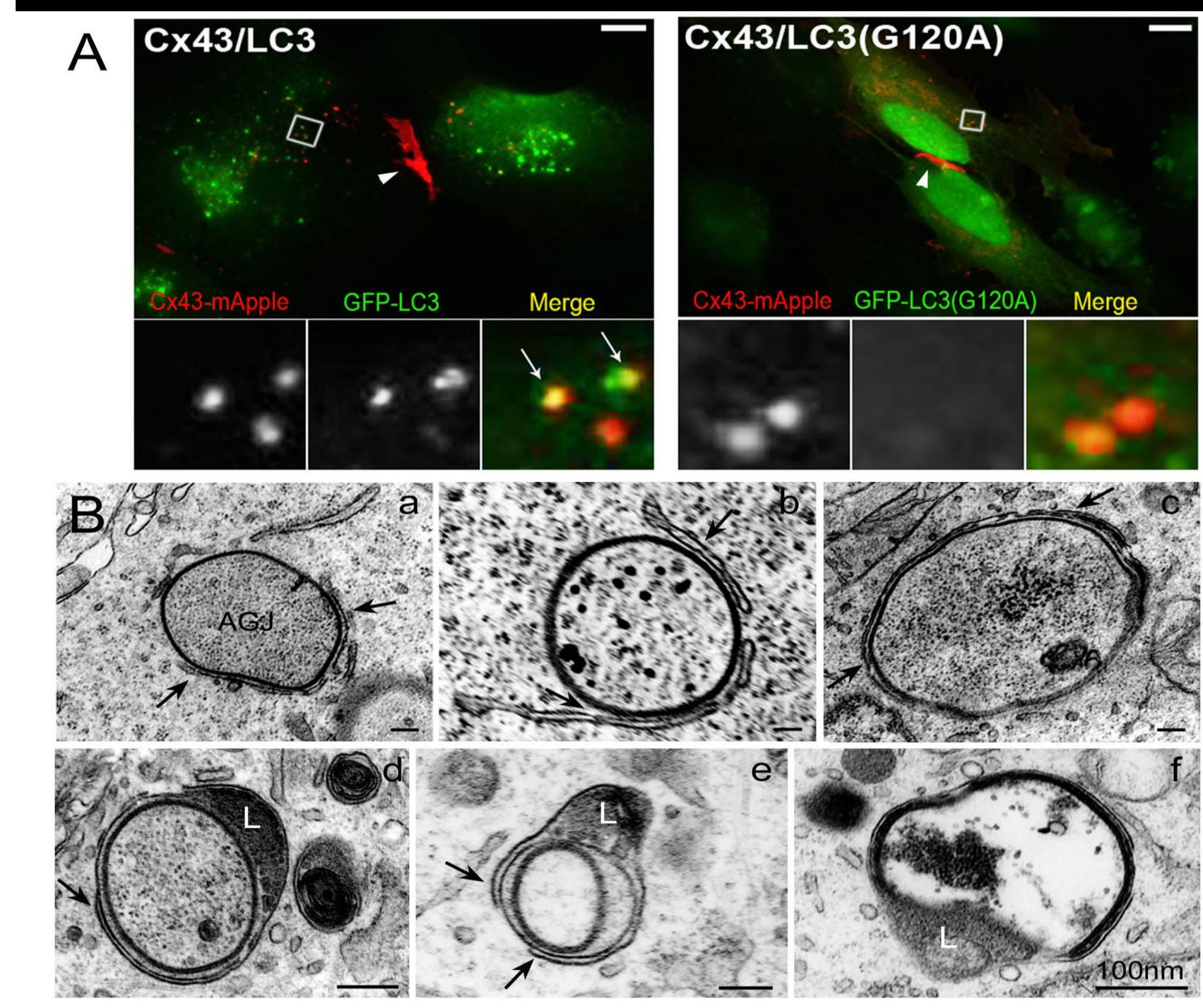

Figure 3: Fluorescence and ultrastructural evidence for autophagic AGJ vesicle degradation. (**A**) HeLa cells were cotransfected with Cx43-mApple and the mammalian autophagy marker protein GFP-LC3 (panel 1), or the activation-deficient LC3-mutant GFP-LC3(G120A) (panel 2). In cells, a fraction of cytoplasmic LC3 (LC3-I) is conjugated to phagophore-membranes (LC3-II) that localizes to autophagosomes; LC3(G120A) cannot be conjugated and remains cytoplasmic. Representative merged fluorescence images acquired 24 hours post transfection are shown. Individual and merged fluorescence signals of the boxed areas are shown below at higher magnification. Robust colocalization of cytoplasmic AGJ vesicles present in Cx43-mApple expressing cells (red puncta) with GFP-LC3-II (green puncta) was observed in GFP-LC3 expressing cells, but not in GFP-LC3(G120A) expressing cells. Representative colocalizing AGJ vesicles are marked with arrows; GJs are marked with arrowheads. Bars = 10 μm. (**B**) Multiple stages characteristic of progressive autophagosome formation and maturation that formed around AGJ vesicles were revealed by ultrastructural analyses of Cx43-GFP expressing HeLa cell preparations. Double-membrane cisternae (isolation membranes, marked with arrows) progressively encircled AGJ vesicles (panels a-c), coalesced into phagophores (panels c-e) and fused with lysosomes (L, panels d, e), resulting in AGJ degradation inside the phagosome (panel f). Strikingly similar ultrastructural images of AGJ/autophagosome-intermediates were also observed *in situ*, in tissues and cells expressing endogenous Cxs (Leach et al., 1984; Pfeifer 1980).

Pharmacological inhibition of autophagy prevents degradation of internalized AGJ vesicles

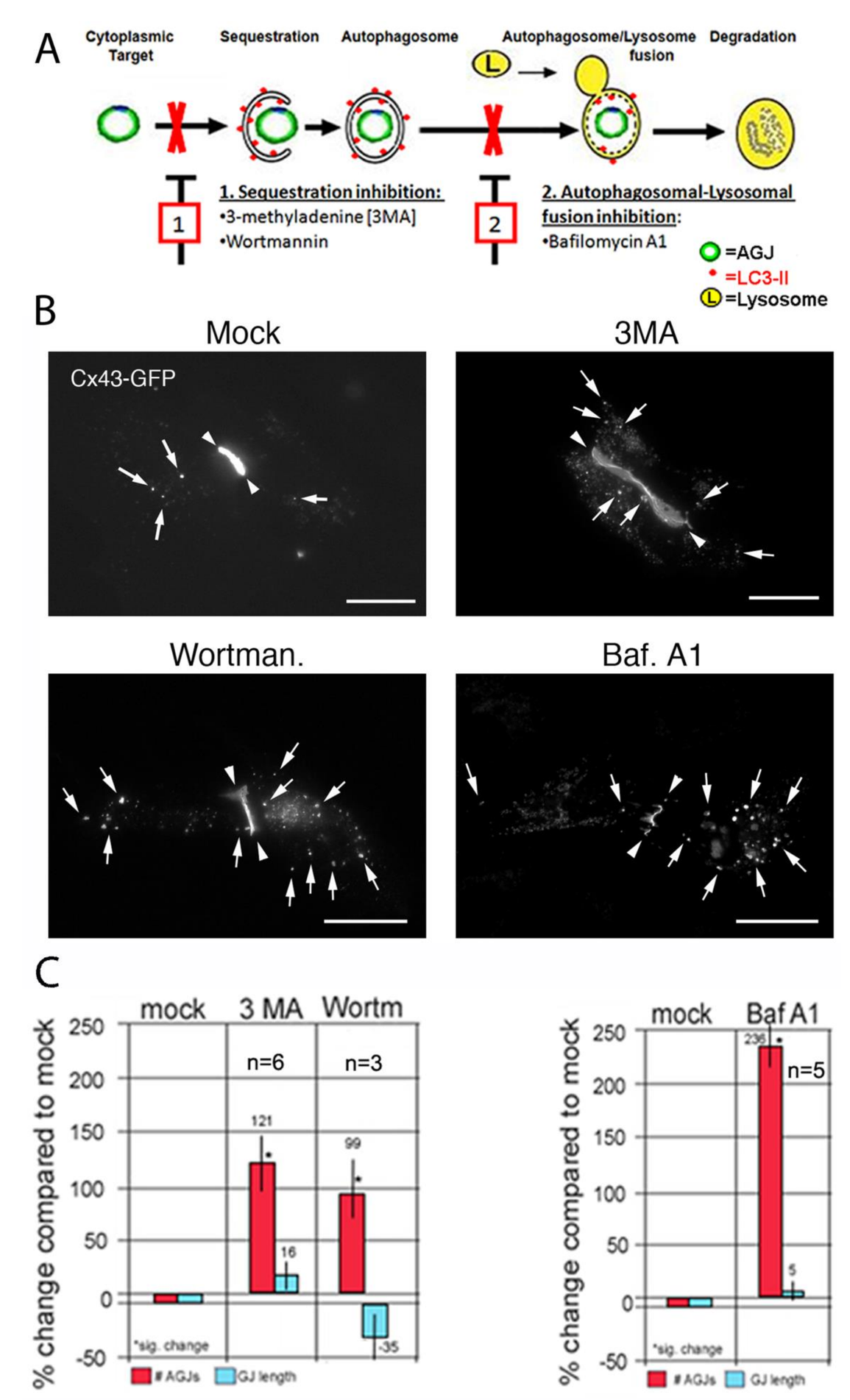

Figure 4 Pharmacological inhibition of autophagic degradation results in the accumulation of AGJ vesicles in the cytoplasm of drug-treated cells. (**A**) Schematic representation of autophagosome-maturation, and of representative steps blocked by drugs used in this study: (**1**), inhibition of cargo sequestration by 3MA and Wortmannin; (**2**), inhibition of autophagosome/lysosome fusion by Bafilomycin A1. (**B**) Fluorescence images of drug-treated and control cells (mock) acquired approximately 21-23 hours post transfection and 5 hours into drug treatments are shown. Representative AGJ vesicles are marked with arrows. GJs are marked with arrowheads. Bars = 20 μm. (**C**) Quantitative analyses of total number of cytoplasmic AGJ vesicles (red columns) and GJ length (blue columns), and compared in percent to mock treated cells are shown. In all drug-treatments, a significant increase in the number of cytoplasmic AGJ vesicles was observed (99, 121, and 236%, marked with asterisks). GJ plaque length was not changed significantly in any of the experiments.

RNAi-mediated knockdown of autophagy-relevant proteins inhibits degradation of internalized AGJ vesicles

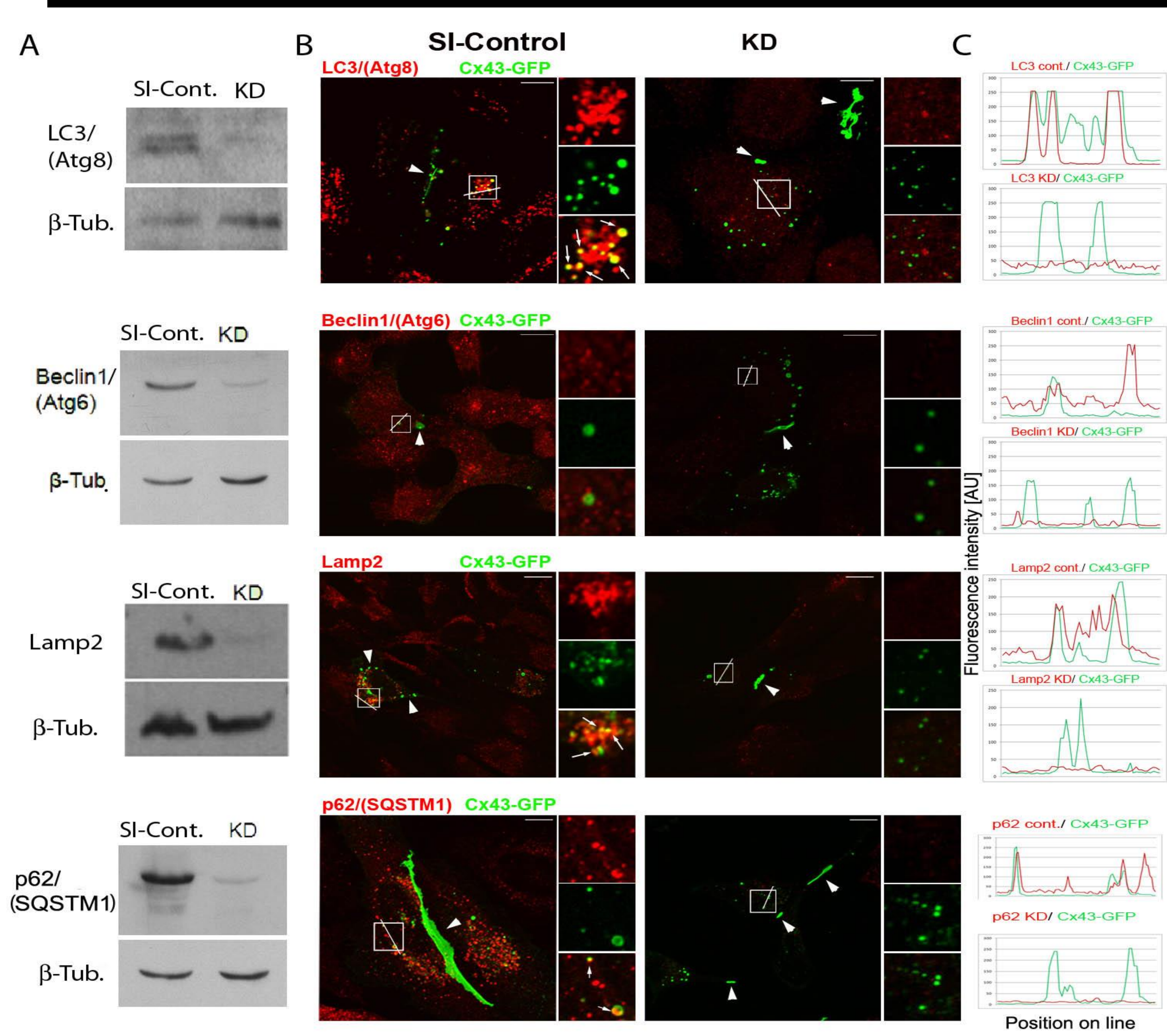

Figure 5: Efficient RNAi-mediated depletion of autophagy-relevant proteins monitored by Western blot and quantitative fluorescence intensity measurements. HeLa cells were transfected with SI-control RNA-oligonucleotides, or with RNA-oligos targeting the autophagy-relevant proteins, LC3/(Atg8), Beclin1/(Atg6), Lamp-2, and p62/SQSTM1 (KD). 48 hours later cells were transfected with Cx43-GFP cDNA and analyzed for KD efficiency 72 hours after oligo transfection. (**A**) Target protein-depletion assayed by Western blot analyses in SI-control and RNAi-KD cells. (**B**) Representative merged confocal fluorescence images of SI-control and KD cells acquired at identical exposure settings are shown. Individual and merged fluorescence signals of the boxed areas are shown at higher magnification on the right. Robust colocalization of Cx43-GFP containing cytoplasmic vesicles was observed with LC3/(Atg8), Lamp-2, and p62/SQSTM1 in mock treated, but not in KD cells (marked with arrows). GJ plaques are marked with arrowheads. Bars = 10 μm. (C) Fluorescence intensities (in arbitrary units) of Cx43-GFP (green) and RNAi-depleted protein (red) for both, SI-control and RNAi-treated cells, measured along lines depicted in (B). Efficient KD of all targeted proteins (>90%) was confirmed by Western blot and quantitative fluorescence line-scan analyses. Beclin1/(Atg6) is known not to efficiently localize to autophagosomes and was not detected to colocalize with AGJ vesicles (B, panel 2). However, a significant cytoplasmic accumulation of AGJ vesicles and reduced AGJ/phagosome colocalization was observed in Beclin1/(Atg6) depleted cells (Figure 6B,C).

RNAi-mediated knockdown of Beclin-1 and p62/SQSTM1-protein significantly reduced AGJ/phagosome colocalization

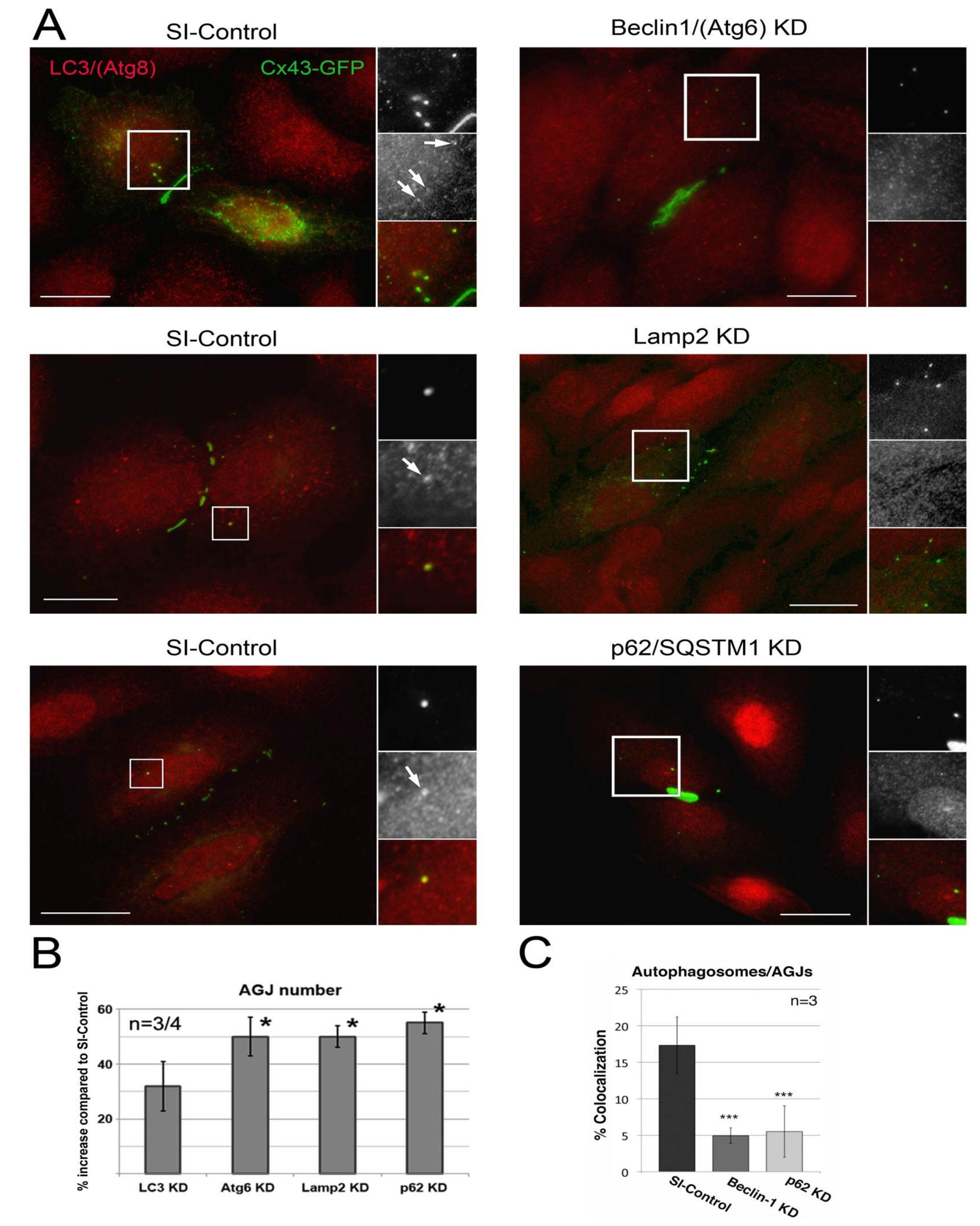

	SI-Control				Beclin1/(Atg6) KD					p62/SQSTM1 KD				
	Total Cell Pairs	Total AGJs	Total Autophago-somes	Total Colocalized	Total Cell Pairs	Total AGJs	Total Autophago-somes	Total Colocalized	% decrease in coloc.	Total Cell Pairs	Total AGJs	Total Autophago-somes	Total Colocalized	% decrease in coloc
Exp. 1	31	324	166	42	27	310	270	13		24	139	157	11	
Exp. 2	35	198	161	37	38	333	138	19		6	56	26	4	
Exp. 3	33	167	175	34	-	-	-	-		10	68	17	1	
Summe	99	689	502	113	65	643	408	32		40	263	200	16	
Av./Cell Pair		Av. AGJs	Av. Autophago-somes	Av. Colocalized		Av. AGJs	Av. Autophago-somes	Av. Colocalized			Av. AGJs	Av. Autophago-somes	Av. Colocalized	
Exp. 1 (%)		10.45	5.35	1.35 (13.0)		11.48	10.0	0.48 (4.2)	67.6		5.79	6.54	0.64 (7.9)	39.0
Exp. 2 (%)		5.66	4.60	1.06 (18.7)		8.67	3.63	0.50 (5.7)	72.0		9.33	4.33	0.67 (7.1)	61.8
Exp. 3 (%)		5.06	5.30	1.03 (20.4)		-	-	-	-		6.80	1.70	0.10 (1.5)	92.8
Av. Exp. 1-3		7.06+/-2.96	5.09+/-0.42	1.15+/-0.18		10.12+/-1.92	6.82+/-4.50	0.49+/-0.01			7.31+/-1.82	4.19+/-2.42	0.41+/-0.29	
(%)				(17.3+/-3.88)				(4.95+/-1.07)	**69.8+/-3.1**				(5.5+/-3.52)	**64.5+/-27.0**
p-value									**<0.001**					**<0.001**

Figure 6: RNAi-mediated depletion of key-autophagic proteins inhibits degradation of AGJ vesicles and decreases the number of AGJ-containing LC3-labled phagosomes. (**A**) HeLa cells were transfected with SI-control RNA-oligonucleotides, or with RNA-oligos targeting the autophagy-relevant proteins, LC3/(Atg8), Beclin1/(Atg6), Lamp-2, and p62/SQSTM1 (KD) as in Figure 5. 48 hours later cells were transfected with Cx43-GFP cDNA and total number of AGJs (in C), and colocalization with LC3-positive phagosomes (in A and B) was analyzed 24 hours later. (A) Beclin1, Lamp-2, and p62 KD and SI-control cells were stained with anti-LC3 antibodies 72 hours post oligo, and 24 hours post Cx43-GFP cDNA transfections. Representative immunofluorescence images are shown. Individual and merged fluorescence signals of the boxed areas are shown at higher magnification on the right. Colocalization of Cx43-GFP AGJ vesicles and LC3-positive phagosomes was observed preferentially in the SI-control cells (marked with arrows). Bars = 20 μm. (**B**) Quantitative analyses of AGJ vesicles, LC3-positive phagosomes, and colocalizing AGJ/phagosomes revealed approximately 17% of colocalizing vesicles in SI control cells, and only approximately 5% in Beclin1 and p62 KD cells (*** = p<0.001) (see Table 1 for total counts). (**C**) Quantitative AGJ vesicle analyses performed 72 hours post oligo transfection indicated a significant cytoplasmic accumulation in Beclin1/(Atg6), Lamp-2, and p62/SQSTM1 depleted cells (≥ 50%, marked with asterisks) compared to SI-control cells. Less pronounced AGJ vesicle-accumulation was observed in LC3-depleted cells (32%), and this was attributed to sufficient inactive LC3-I that may remained in the LC3-KD cells and may have been converted into active LC3-II.

LC3 and p62/SQSTM1 colocalize with endogenous Cx43 in primary PAE cells

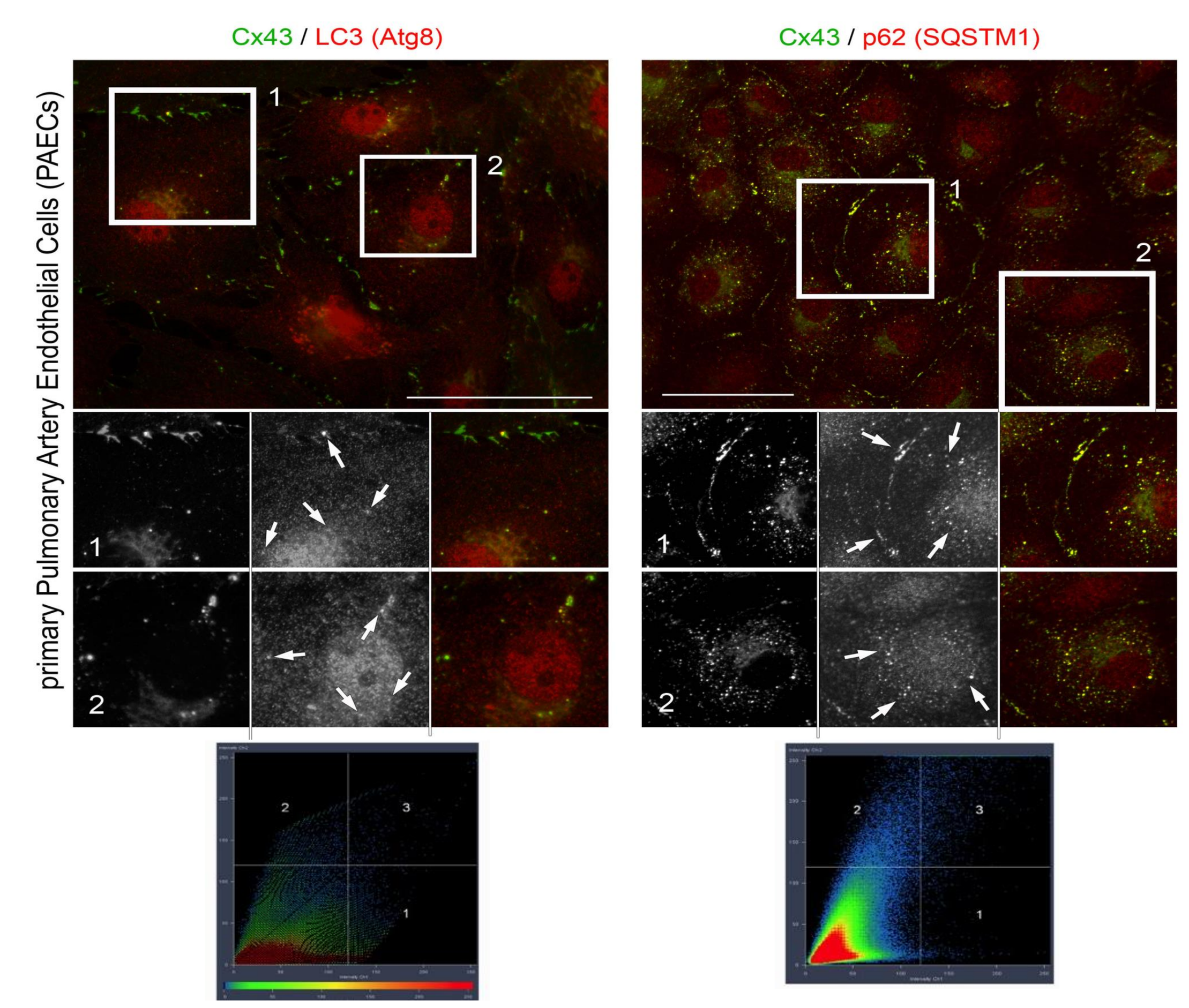

Figure 7: LC3 and p62/SQSTM1 protein colocalize with endogenously expressed Cx43-based GJs and AGJ vesicles. Endogenously Cx43 expressing porcine primary pulmonary artery endothelial cells (PAECs) were stained for Cx43, LC3, and p62/SQSTM1 using specific mono and polyclonal antibodies, and potential Cx43-LC3/p62 colocalization was qualitatively and quantitatively analyzed. (**A**) Representative merged fluorescence images of confluent PAECs are shown. Individual and merged fluorescence signals of the boxed areas are shown below at higher magnification. Significant colocalization of LC3 with AGJ vesicles, and of p62 with AGJ vesicles and individual plasma membrane GJs was observed, even at stringent threshold settings (marked with arrows). Bars = 20 μm. (**B**) Quantitative scatter-blot colocalization analyses of the images shown in (A) with applied maximum intensity threshold settings of 120 (of maximum 250 arbitrary units; white lines) indicated.

Conclusions

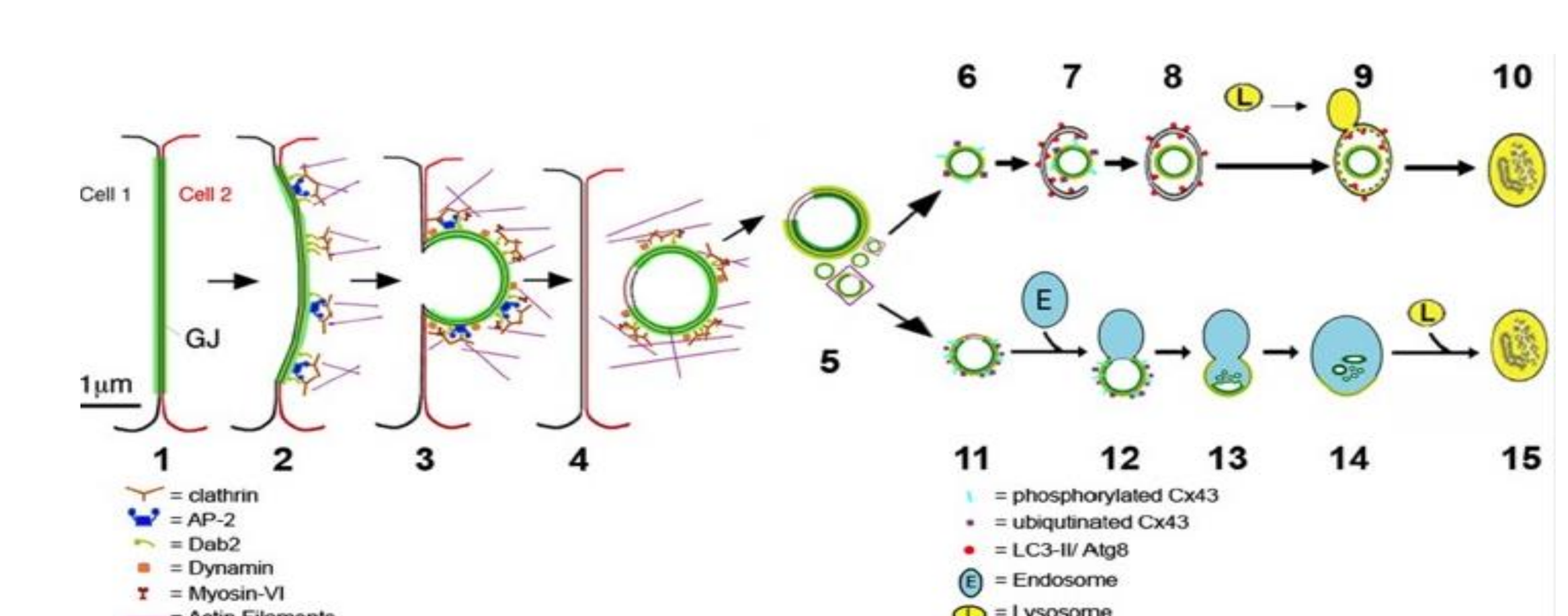

Figure 8: Schematic representation of the proposed steps that lead to GJ internalization (1-3), AGJ vesicle formation and fragmentation (4, 5), and AGJ vesicle degradation by phago-/lysosomal (6-10) and endo-/lysosomal (11-15) pathways based on the present and previous work by others and us. In conclusion, our analyses provide molecular and mechanistic insights into a GJ degradation pathway that previously had not significantly been appreciated. Its recent link to health and disease lends further importance to this GJ degradation pathway. Another recent study also reports that autophagy contributes to Cx43 and Cx50 degradation, in wild-type as well as in cells in which autophagy was induced by starvation (Lichtenstein et al. 2011). In addition, our work adds to the growing consensus that autophagy plays an important role as a normal cellular degradation pathway, rather than representing solely a rescue pathway designed to supply critical nutrients during starvation.

References & Acknowledgements

-- Piehl M, Lehmann C, Gumpert A, Denizot JP, Segretain D, Falk MM. Mol Biol Cell 2007; 18:337-47; -- Gumpert AM, Varco JS, Baker SM, Piehl M, Falk MM. FEBS Lett 2008; 582:2887-92; --Baker SM, Kim N, Gumpert AM, Segretain D, Falk MM. FEBS Lett 2008; 582:4039-46; --Gilleron J, Fiorini C, Carette D, Avondet C, Falk MM, Segretain D, Pointis G. J Cell Sci 2008; 121:4069-78; --Hesketh GG, Shah MH, Halperin VL, Cooke CA, Akar FG, Yen TE, Kass DA, Machamer CE, Van Eyk JE, Tomaselli GF. Circ Res 2010; 106:1153-63; --Leach DH, Oliphant LW. Acta Anat (Basel) 1984; 120:214-9; --Pfeifer U. Eur J Cell Biol 1980; 21:244-; --Lichtenstein A, Minogue PJ, Beyer EC, Berthoud VM. J Cell Science 2011; 124:910-920.

We thank T. Yoshimori (National Institute of Genetics, Shizuoka, Japan) for providing fluorescent LC3 constructs; J.-P. Denizot (Unite de Neurosciences Integratives et Computationnelles, CNRS, Gif sur Yvette, France) for the preparation of ultra-thin sections; and D. Segretain (Institut National de la Sante et de la Recherche Medicale U895, Universite Paris Descartes, 75006 Paris, France) for ultrastructural examination of our Cx43-GFP expressing HeLa cell samples. This work was supported by NIHs NIGMS (grant GM55725 to MMF).